Fast Spectrum Shaping for Next-Generation Wireless Networks

Eugene Chai, *Student Member*, *IEEE*, Kang G. Shin, *Life Fellow*, *IEEE*, Jeongkeun Lee, *Member*, *IEEE*, Sung-Ju Lee, *Fellow*, *IEEE*, and Raúl H. Etkin, *Senior Member*, *IEEE*

Abstract—Spectrum management and device coordination for dynamic spectrum access (DSA) networks have received significant research attention. However, current wireless devices have yet to fully embrace DSA networks due to the difficulties in realizing spectrum-agile communications. We address the practical hurdles and present solutions toward implementing DSA devices, answering an important question "what is a simple practical extension to current wireless devices that makes them spectrum-agile?" To this end, we propose RODIN, a general per-frame spectrum-shaping protocol that has the following features to support DSA in commercial off-the-shelf (COTS) wireless devices: 1) direct manipulation of passband signals from COTS devices, 2) fast FPGA-based spectrum shaping, and 3) a novel preamble design for spectrum agreement. RODIN uses an FPGA-based spectrum shaper together with a preamble I-FOP to achieve per-frame spectrum shaping with a delay of under $10\ \mu$s.

Index Terms—Software-defined radio, hybrid radio, spectrum agility, per-frame spectrum shaping, spectrum-agile preamble detection

1 Introduction

Dynamic spectrum access (DSA), or spectrum agility, has become a popular solution to the problem of spectrum scarcity in wireless networks [6]. New devices that are designed to use only a monolithic block of spectrum can no longer expect to increase throughput by simply increasing their bandwidth. In fact, the throughput of an 802.11n device operating at 40 MHz can even be *lower* than its throughput at 20 MHz when encountering a 20-MHz interference from another 802.11 g or 802.11n device [8], [22]. Numerous other studies [12], [18] have reported performance anomalies when rate or bandwidth is blindly increased in an attempt to wrest more throughput from an overcrowded spectrum. We can only expect such problems to compound with the introduction of 802.11ac that support up to 160-MHz bandwidth. While this example deals with Wi-Fi networks for clarity in exposition, the infeasibility of enhancing throughput by merely increasing bandwidth is also prevalent in non-Wi-Fi networks. For example, a study of GSM usage patterns [15] shows that a wideband device cannot operate within the GSM band without some form of spectrum agility.

However, despite this obvious problem and the list of well-studied solutions, building efficient spectrum-agile devices is still a challenge for two main reasons. First, the current crop of commercial wireless devices is ill suited for DSA networks as they are primarily designed to use static, monolithic spectra. For example, spectrum- and bandwidth-agile platforms, such as SampleWidth [5] and FLUID [20], all have channel-switch times on the order of milliseconds. Second, the protocol stack does not fully support spectrum-agile communications. As an example, consider 802.11n OFDM frames that are detected by exploiting the self-correlation property of the preamble. This approach fails if the preamble is spread out over a noncontiguous spectrum, or in the face of interference from narrower band devices. Noncontiguous OFDM (NC-OFDM) techniques can be applied, but synchronization can be performed if and only if the set of noncontiguous subcarriers is known at the receiver beforehand.

We argue that the key capability that is missing from current state-of-the-art radio hardware is per-frame spectrum shaping. This is an important functional primitive that allows a radio to adapt to challenging channel conditions at the smallest practical unit of transmission.

1.1 Why Per-Frame Spectrum Shaping?

1.1.1 Wi-Fi Channels

802.11 devices are known to suffer significant performance degradation due to narrowband interference [11]. The effects of narrowband interference include timing recovery failure, the automatic gain control (AGC) failure due to an unexpected introduction of interference energy, and Physical Layer Convergence Protocol (PLCP) header processing failure.

Rapid frequency hopping (FH) by an 802.11 device [11] has been shown to improve its performance in the presence of narrowband interference. However, FH cannot avoid interference from a FH interferer, such as Bluetooth, if the hopping sequences of the Wi-Fi and the interferer are not properly synchronized. Furthermore, collision between multiple FH devices using different hopping sequences is a well-known challenge when scaling FH to a larger network [17].

- *E. Chai and K.G. Shin are with the Department of Electrical Engineering and Computer Science, The University of Michigan, 2260 Hayward St., Ann Arbor, MI 48109. E-mail: {zontar, kgshin}@eecs.umich.edu.*
- *J. Lee is with Hewlett-Packard Laboratories, 1501 Page Mill Road, M/S 1184, Palo Alto, CA 94304. E-mail: jklee@hp.com.*
- *S.-J. Lee is with Narus, Inc., Office of the CTO, 570 Maude Court, Sunnyvale, CA 94085. E-mail: sjlee@narus.com.*
- *R.H. Etkin is with Samsung Information Systems America, San Jose, CA 95134. E-mail: raul.etkin@samsung.com.*

Manuscript received 15 Nov. 2012; revised 27 July 2013; accepted 15 Aug. 2013; published online 27 Sept. 2013.
For information on obtaining reprints of this article, please send e-mail to: tmc@computer.org and reference IEEECS Log Number TMCSI-2012-11-0562. Digital Object Identifier no. 10.1109/TMC.2013.125.

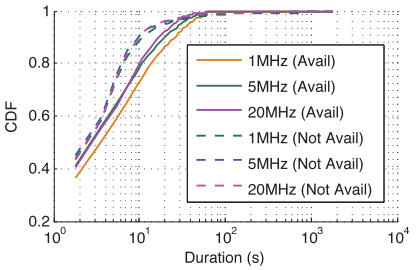

Fig. 1. CDF of the channel busy and available durations in non-Wi-Fi frequency bands.

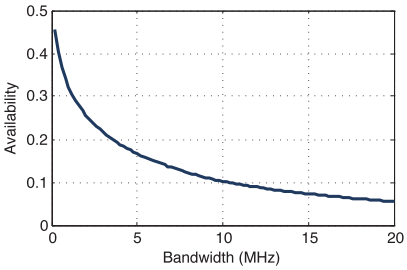

Fig. 2. Channel availability of different transmission bandwidths.

This disadvantage of FH comes from the fact that it switches channels blindly, even when there is no interference on the channel it is currently using. This increases the possibility of the FH itself interfering with devices on other channels. We posit that a reactive approach to interference avoidance using per-frame spectrum shaping will enable 802.11 devices to avoid narrowband interference while maintaining high throughput and manageability. The use of per-frame spectrum shaping effectively reallocates the spectrum of a transmission dynamically only when interference is detected on the channel. This minimizes the amount of spectrum touched by an 802.11 device and avoids the unnecessary channel-switch overhead when no interference is detected.

1.1.2 Non-Wi-Fi Channels

Devices operating in non-Wi-Fi channels have to contend with severe spectrum fragmentation due to multiple narrowband interferers. We illustrate this using spectrum traces [29] that took measurements from a 1.5-GHz band and is centered at 770-MHz frequency. This trace set, thus, covers multiple GSM and TV channels.

Fig. 1 shows the availability and outage durations of 1-, 5-, and 20-MHz monolithic channels operating within this band. Consider, in particular, the 20-MHz transmission that is typical of Wi-Fi devices. At a first glance, the long median channel-availability duration of 3 s can easily accommodate the channel-switch time of typical Wi-Fi devices. However, we observe from Fig. 2 that monolithic 20-MHz channels can transmit only about 6 percent of the time. This low availability is due to the presence of multiple uncoordinated narrow bandwidth interferers. Hence, to sustain a 20-MHz transmission, multiple discontiguous 1-MHz (or narrower) channels have to be bonded together. Given that the correlation between the different channels is low [15], such a device can expect to continuously reconfigure its set of bonded channels to avoid primary user interference. The otherwise long outage duration that it faces, as shown in Fig. 1, will severely degrade the quality of service. The ability to perform per-frame spectrum shaping is, thus, key for operating in non-Wi-Fi channels as well.

1.2 The Limitation of SDRs

Software-defined radios (SDRs) have been used to develop the flexible RF interfaces required for DSA devices. However, SDR platforms face problems arising from poor efficiency and high complexity. SDR platforms, such as USRP [27] and SORA [26], are limited by the efficiency of a general-purpose platform in multitasking real-time DSP with other system tasks, while FPGA-based SDR platforms, such as WARP [28], are complex to work with. This complexity and inefficiency poses a significant challenge because it is necessary to reimplement the entire MAC/PHY protocol on the SDR platform to reap the advantage of PHY-layer flexibility.

1.3 The Limitation of COTS Devices

A commercial off-the-shelf (COTS) device that has its RF frontend separated from the MAC baseband chipset can facilitate easy integration between the SDR and COTS. However, COTS devices are increasingly implemented as single-chip solutions to improve power and space efficiency. This limits the flexibility of the RF frontends of COTS devices in supporting the various spectrum management policies required for per-frame spectrum shaping.

1.4 The Challenge

We take a very different approach to DSA and address an important question: *"What is a simple practical extension to current wireless devices that makes them spectrum agile?"* We stress that any solution must be *general* enough to apply to the majority of COTS wireless devices currently available, yet *simple* enough to minimize the additional overhead that are added to COTS devices.

The intuition behind this comes from the fact that neither COTS devices nor SDRs are individually capable of supporting the per-frame spectrum shaping necessary for DSA. Hence, a hybrid platform built using both SDRs and COTS devices is necessary. The SDR handles only the necessary PHY-layer manipulations, while the COTS device handles the main MAC/PHY processing. A practical DSA extension must have the following three important properties.

Property 1: Protocol Independence. It must support as many current wireless protocols as possible. Hence, a COTS device should only have to be "plugged into" a DSA extension platform to gain spectrum agility. In reality, some modifications to the COTS platform may be necessary, but such changes must be minimal. Easy deployability of a DSA extension platform will naturally maximize the chance of its widespread acceptance. With this property, RODIN can be easily integrated into both OFDM and non-OFDM COTS devices.

Property 2: Per-frame spectrum shaping. Per-frame spectrum shaping is a general spectrum-shaping primitive that can be used to construct other spectrum-management protocols. In the absence of detailed knowledge about the behavior of other devices in the ISM or whitespace bands, a DSA platform must be able to adjust its spectral use on

a frame-by-frame basis to react to unexpected transmissions by primary users.

Property 3: Fast spectrum agreement. Besides having the capability of per-frame spectrum shaping, the transmitter and receiver(s) must also agree on a common set of (possibly noncontiguous) spectrum bands before commencing transmission. Prior work on spectrum agreement made use of control channels [31], predefined backup channel lists [23], or centralized channel assignment [20]. Unfortunately, these approaches are too slow to meet the required delay bounds for per-frame spectrum shaping.

1.5 Rodin: Our Solution

We propose RODIN[1]—a hardware DSA extension to COTS devices. RODIN consists of three key components that enable it to serve as a drop-in DSA extension to arbitrary wireless devices.

Direct connection to COTS device. RODIN connects to a COTS device directly through the antenna port(s) on the COTS radio, thus upgrading unmodified COTS devices with spectrum agility.

Fast FPGA-based spectrum shaping. RODIN can split the spectrum of an unmodified signal from the COTS device into multiple noncontiguous spectrum subbands; the individual subbands are transmitted on unoccupied portions of the spectrum to avoid interference from other narrowband transmitters. RODIN does not decode the signals to and from the COTS device. Our hardware implementation achieves this spectrum subdivision of each frame within 2 μs of detecting a passband signal from the COTS device.

Novel preamble design for spectrum agreement. A RODIN transmitter uses a novel preamble design to notify a RODIN receiver of the spectrum occupied by the accompanying spectrally reshaped frame. With this preamble, RODIN eliminates the need for a separate control channel, backup channel lists or a centralized spectrum coordinator. This preamble, when combined with fast spectrum shaping, enables RODIN to rapidly adapt to any primary transmission pattern seen on channels.

To see how efficiently this can be done, consider shaping a 20-MHz 802.11n frame over multiple 5-MHz subbands. Spectrum agreement and shaping can be achieved in under 10 μs. This adds only 3.8 percent of additional overhead to the transmission time of an 802.11n frame without aggregation. The overhead will be even lower if frame aggregation is used. The negligible overhead enables RODIN to react to rapidly changing channel conditions on all types of channels.

RODIN is a novel RF front end for COTS devices for cognitive spectrum management. In the short term, it extends the experimental capabilities of COTS devices but it can also be built into COTS devices to achieve integrated SDR-COTS hybrids in the future.

Our contributions in this paper are: 1) a detailed design of spectrum shaping and agreement in RODIN, 2) an evaluation of the real-world performance of RODIN via controlled experiments with FPGA-based implementations, and 3) an analysis of the performance of RODIN using detailed channel measurements.

1. Named after Auguste Rodin, the French sculptor.

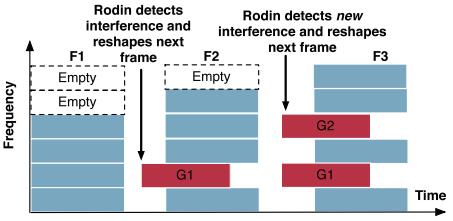

Fig. 3. Transmission of three frames F_1, F_2, and F_3 using RODIN. RODIN reshapes the spectrum of F_2 and F_3 to avoid interference from G_1 and G_2, respectively.

2 Overview of Rodin

RODIN is a general-purpose per-frame spectrum-sculpting platform designed for wideband frame-based COTS devices. In particular:

- RODIN is designed for wideband COTS devices that share the spectrum with other devices of narrower bandwidth. Examples of such scenarios include 160-MHz 802.11ac or 40-MHz 802.11n devices that share the same 5-GHz band with 802.11a devices operating at 20 MHz; UWB devices that share the spectrum with narrowband cellular networks.
- RODIN assumes that the maximum bandwidth of its SDR RF front end is greater than the bandwidth of the transmitted COTS signal. RODIN shapes the spectrum of each frame while keeping the overall transmission bandwidth constant. Note that RODIN does not change the operating bandwidth of the COTS device.
- RODIN is designed for CSMA networks with multiple concurrent asynchronous transmitters that occupy nonoverlapping spectra. This maximizes the frequency reuse of wireless channels. However, these channels are not perfectly orthogonal to each other due to nonideal pulse shaping filters [16].

RODIN has three key features to function as a general per-frame spectrum-shaping platform for COTS devices: 1) capability for direct connection to the COTS device, 2) FPGA-based spectrum shaping, and 3) a novel preamble design for fast spectrum agreement.

RODIN divides its total RF bandwidth B into N subbands and shapes the spectrum of a frame that occupies N_F ($< N$) of these subbands. Fig. 3 shows an example of RODIN reshaping a wideband transmission, with $N = 6$ and $N_F = 4$, in the face of narrowband interference. Frame F_1 can be transmitted without any additional shaping because no interfering transmission is present. However, almost immediately after transmitting F_1, RODIN detects a narrowband interference G_1 that occupies one subband. It maps the spectrum of F_2 into the remaining subbands and transmits it without interfering with G_1. This frame-by-frame spectrum reshaping is repeated for F_3 to avoid interference from G_2.

If per-frame spectrum shaping is not used, a wideband transmission would be blocked by a narrowband transmission, or a wideband transmission collides with a narrowband transmission if the narrowband transmitter does not correctly detect the wideband transmission.

These features are realized with the system architecture shown in Fig. 4. The *spectrum shaper* reshapes the signal to

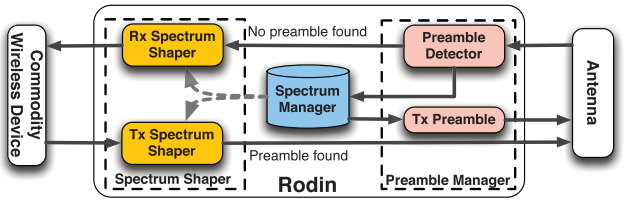

Fig. 4. High-level architecture of RODIN.

and from the COTS wireless device in real time, while the *preamble manager*, consisting of a preamble detector and a preamble constructor, uses specially constructed preambles to exchange spectrum information between RODIN devices. The *spectrum manager* executes a protocol that selects the best set of spectrum bands for a particular transmitter-receiver pair.

These components are detailed in the rest of this paper. For simplicity, our current design of RODIN is limited to SISO devices only, although an extension to MIMO devices is straightforward.

3 Spectrum Shaping in Rodin

Spectrum shaping divides the spectrum occupied by a COTS device into multiple discontiguous frequency bands. To realize real-time spectrum shaping, 1) the spectrum-shaping procedure must have low latency and 2) the spectrum shapers on the transmitter and the receiver must cooperate with minimal synchronization. Property 1 relates to the efficiency of the spectrum shaper—upon specification of the desired subbands, the shaper must quickly reshape the spectrum with minimal delay. In contrast, Property 2 relates to the tolerance of the spectrum shaper to errors caused by channel distortion, timing, frequency shifts, and so on. This is particularly important because different PHY protocols engage different measures to combat distortions. For example, DSSS-based protocols use Rake receivers and equalizers, while OFDM-based protocols use the Schmidl-Cox algorithm. Obviously, it is not feasible for RODIN to support the wide variety of synchronization primitives to achieve protocol independence. Hence, RODIN focuses on spectrum shaping while leaving protocol-specific DSP functions (such as pilot handling) to the COTS device.

In the rest of this section, we only describe a two-band shaping process ($N > N_F = 2$) for the sake of clarity. This process can be easily extended to multiband shaping.

3.1 Overview of Spectrum Shaping

Let $X(f)$ denote the original spectrum of the frame received by RODIN from the attached wireless device. The spectrum-shaping procedure for the frame *transmission* consists of the following components:

1. *Prefilter modulation.* RODIN only uses low-pass filters for spectrum shaping. Hence, the input signal $X(f)$ must be modulated to align the relevant portion of $X(f)$ with the passband of the filter $H(f)$. Let $m_1^{(a)}(t) = \exp\{j2\pi k_1 Bt/N\}$ and $m_2^{(a)}(t) = \exp\{j2\pi k_2 Bt/N\}$ be the time-domain complex-valued carrier used to modulate $X(f)$, with $k_i = 0, \ldots, N-1, \forall i = 1, 2$. The modulated spectrum is

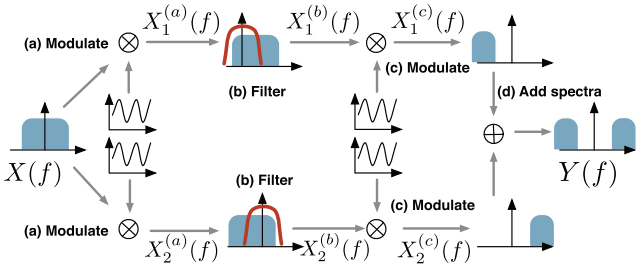

Fig. 5. Shaping a frame occupying a contiguous spectrum $X(f)$ into two separate spectrum bands $Y(f)$. The shaping procedure is a four-step process, labeled (a)-(d).

$$X_i^{(a)}(f) = X(f) * \delta(f - k_i B/N) = X(f - k_i B/N),\ \forall i = 1, 2, \quad (1)$$

where $\delta(\cdot)$ is the Dirac delta function.

2. *Filtering.* Once the spectrum of the input signal has been appropriately modulated, a low-pass filter is applied to split the input spectrum into two separate subbands. Let $H_1(f)$ and $H_2(f)$ be the two low-pass filters used in this example. The two spectral subbands $X_1^{(b)}(f)$ and $X_2^{(b)}(f)$ are

$$X_i^{(b)}(f) = H_i(f) X_i^{(a)}(f) = H_i(f) X(f - k_i B/N), \forall i = 1, 2. \quad (2)$$

3. *Postfilter modulation.* Each filtered subband must be transmitted at a frequency that encounters minimum interference. This modulation step uses $m_1^{(c)}(t) = \exp\{j2\pi l_1 Bt/N\}$ and $m_2^{(c)}(t) = \exp\{j2\pi l_2 Bt/N\}$ as the modulating carrier, where $l_1, l_2 = 1, \ldots, N$. The second modulation step achieves $\forall i = 1, 2$:

$$X_i^{(c)}(f) = X_i^{(b)}(f) * \delta(f - l_i B/N) = X_i^{(b)}(f - l_i B/N) = H_i(f - l_i B/N) X(f - (l_i + k_i) B/N). \quad (3)$$

4. *Combining spectra.* Finally, the two subbands are added to produce a single spectrally noncontiguous frame. This results in a single time-domain data stream that is sent to the radio front end of RODIN to be transmitted:

$$Y(f) = X_1^{(c)}(f) + X_2^{(c)}(f). \quad (4)$$

The RODIN *receiver* executes the same process as shown in Fig. 5 using the same low-pass filters but with the modulation sinusoids rearranged as

$$X(f) = \hat{Y}(f), Y(f) = \hat{X}(f),$$
$$m_1^{(a)}(t) = 1/m_1^{(c)}(t), m_2^{(a)}(t) = 1/m_1^{(c)}(t),$$
$$m_1^{(c)}(t) = 1/m_1^{(a)}(t), m_2^{(c)}(t) = 1/m_1^{(a)}(t),$$

where $\hat{Y}(f)$ is the spectrum of the received frame and $\hat{X}(f)$ is the spectrum of the reconstructed frame.

3.2 Filter Design for Spectrum Shaping

Prior work in spectrum shaping has largely adopted an OFDM-based approach [25], [30], [32]. While this approach draws upon many readily understood concepts similar to

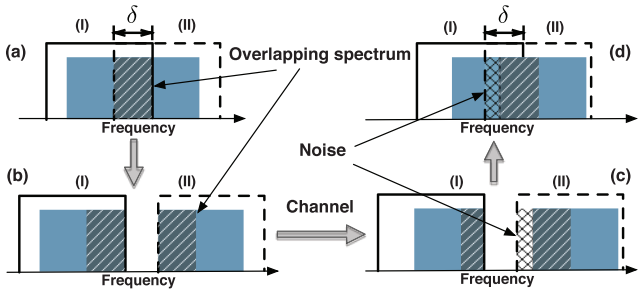

Fig. 6. Spectrum shaping using two partially overlapping filters. (a) Two subbands share an overlapping band δ. (b) After postfilter modulation, each subband contains a copy of the overlapping spectrum δ. (c) As a result of frequency drift at the receiver, only a portion of one subband is recovered while the other subband is recovered along with a noise band. (d) The overlapping spectrum δ ensures that the original spectrum can be reconstructed even if one subband is not recovered completely.

typical OFDM(A) modulation schemes, it has two significant disadvantages when applied to real-time spectrum shaping: 1) high overhead and complexity involved in maintaining strict time and frequency synchronization with pilot subcarriers, and 2) reduction in throughput due to the necessary use of a cyclic prefix to guard against intersymbol interference.

RODIN mitigates these disadvantages with partially overlapping finite-impulse response (FIR) spectrum shaping filters. Note that these FIR filters are only used for spectrum shaping. RODIN can support both OFDM and non-OFDM protocols using these FIR filters. RODIN itself is tolerant of timing drifts as time synchronization is handled by the attached COTS device as part of its PHY protocol; as long as the filtered spectrum encompasses the received frame, the COTS device can determine the appropriate frame boundary. RODIN is also resilient to frequency drifts by transmitting redundant spectral information through the use of partially overlapping filters.

To understand this, consider the use of partially overlapping filters to shape an input frame, as illustrated in Fig. 6. The two filters divide the spectrum into two portions, (I) and (II), that share a common overlapping subband of bandwidth δ, as shown in Figs. 6a and 6b. A frequency shift at the receiver, as shown in Fig. 6c, causes some spectrum to be lost from (I) and noise to be introduced into (II). Observe that when the two subbands are recombined, the spectral information missing from (I) can be recovered from its redundant copy in (II). The degree of resilience to frequency drift is governed by the overlapping bandwidth δ, which is a configuration parameter. We must ensure that the value chosen for δ is greater than the expected frequency drift. The lower bound on the overlapping bandwidth, thus, depends on the quality of the COTS device that RODIN is connected to. The effect of this noise is minimal because it is located at the very edge of the shaping filter and thus will be more heavily attenuated. Furthermore, this noise subband is typically very narrow as real-world measurements of actual frequency drift are shown to be small [4].

The overlapping bandwidth is also lower bounded by the amount of resources available on the FPGA: longer filters, which allow smaller overlapping bandwidths, require larger numbers of FPGA slices. The WARP platform used for our RODIN prototype can support a 64-tap filter.

The ideal requirements for a spectrum shaping filter are: 1) constant unit amplitude response and linear phase response in the passband, 2) narrow transition bandwidth, and 3) very high attenuation in the stopband. Unfortunately, neither the typical windowed approach nor the Parks-McClellan algorithm can produce a filter that satisfactorily meets these three constraints. Thus, we adopt a *constrained least squares* algorithm [21] for filter design. We design our filters, using this algorithm, to have 64 taps, a passband ripple of 0.1 dB and an overlapping spectrum bandwidth that is approximately 10 percent of the total filter bandwidth.

3.3 Spectrum-Shaping Latency

We have implemented the spectrum shaper using a 64-tap FIR filter on the FPGA of the WARP platform to both validate its functionality and study the latency incurred in real-time spectrum shaping. The FPGA on the WARP runs at 40 MHz.

The modulation and spectral combination steps consist of time-domain multiplication and addition, respectively. Each step, thus, incurs a latency of one clock cycle. The filtering step consists of a 64-tap time-domain convolution, and incurs a latency of 64 cycles. Note that the filtering latency is *independent* of the number of subbands used because all filters run in parallel on the FPGA.

The total latency of real-time spectrum shaping is, therefore, $64 + 1 + 1 = 66$ cycles, or $1.65\ \mu s$ when running on the 40-MHz FPGA. This spectrum-shaping latency is a mere 0.7 percent of the transmission time of a 1.5-KB 802.11n frame sent at 54 Mbps (Rodin currently only supports SISO). Hence, a real-time spectrum shaping extension to commodity wireless hardware is feasible.

4 Preamble for Spectrum Agreement

RODIN uses a unique preamble that is designed to indicate both the start of a frame as well as the spectrum bands it occupies.

4.1 Challenges to Spectrum Agreement

A frame sent by the transmitter can be decoded if and only if the spectrum occupied by the frame is known by the receiver. If the spectrum occupancy of a frame is unknown, the receiver can attempt to search for the frame over all the subbands. Assuming that a frame is known to occupy M out of N subbands, the receiver has to attempt to search for the frame over $N!/(M!(N-M)!)$ possible subband combinations; if the bandwidth of the frame is unknown, this search space increases to $\sum_{m=1}^{M} N!/(m!(N-m)!)$ subband combinations.

One might think of applying energy sensing to the subbands and decoding a frame using only the subbands with signal energy above a given threshold. This method, though simple, suffers from two serious limitations: 1) frequency-selective fading on the subband may result in a missed detection, and 2) in the case of multiple concurrent transmissions, each using a different set of subbands, it is impossible for a receiver to correctly map each occupied subband to its transmitter based on energy detection alone.

4.2 I-FOP Design

RODIN addresses this predicament by prepending a multi-subband preamble, In-Front of Preamble (I-FOP), to the transmitted COTS frame. A unique preamble is assigned to each *flow* within the network, where a flow is simply a group of consecutive frames sent by the COTS device. This preamble must, therefore, be designed to 1) assign an address to each unique flow within the network, 2) specify the subband occupancy of each transmitted frame, and 3) enable the receiver to recover both the address and subband occupancy information of each frame without prior coordination with the transmitter. We stress that the spectrum occupancy can change from frame to frame even within the same flow.

A key feature that the preamble must possess is a strong correlation property—a receiver searching for a preamble P via correlations must encounter a large correlation peak if and only if P is present on the channel. Furthermore, this autocorrelation property must hold for a large set of sequences of the same length. This allows a different preamble to be assigned to each flow within a collision domain.

Zadoff-Chu (ZC) sequences [7] meet our requirements and are, thus, used in I-FOP. The length-L discrete ZC sequence is

$$x_u[n] = \exp\left(-j\frac{\pi un(n+1)}{L}\right), \tag{5}$$

where u is the sequence ID and $0 \leq n, u \leq L-1$. ZC sequences have strong correlation properties that make them ideal for I-FOP: 1) the autocorrelation of a length-L ZC sequence with a cyclically shifted version of itself is zero if L is prime; and 2) the cross correlation between two prime length ZC sequences is $1/\sqrt{L}$.

RODIN selects a set $\{p_0, \ldots, p_{N_F-1}\}$ of ZC sequences to address a flow. The bandwidth of each frame within the flow occupies N_F subbands. RODIN applies a random cyclic shift to each sequence before constructing the preamble for the flow. The cross-correlation property reduces the chance of collision in the event that the same ZC sequence is selected by multiple transmitters. With this approach, there is a large set of L^2 ZC sequences of length-L that can be used to construct preambles.

Let $\mathbf{f} = \{f_0, \ldots, f_{N_F-1}\}$ be the set of N_F subbands that RODIN uses to transmit a frame. The preamble constructed for this particular frame is specified by the set $\mathbf{S} = \{S_{f_k}^{p_k} : 0 \leq k \leq N_F - 1\}$, where $S_{f_k}^{p_k}$ indicates that sequence p_k is transmitted on the subband f_k and $f_0 \leq \cdots \leq f_{N_F-1}$. The time-domain representation of the preamble is

$$y[n] = \sum_{k=0}^{N_F-1} x_{p_k}[n] \cdot e^{-j2\pi f_k n/N} \tag{6}$$

for $0 \leq n \leq L-1$.

4.3 I-FOP Detection

We assume, for now, that the transmitter and the receiver know the set of ZC sequences, $\{p_0, \ldots, p_{N_F-1}\}$, used to address the flow between them. The receiver faces the challenge of determining the set of subbands $\{f_0, \ldots, f_{N_F-1}\}$ occupied by the transmitted frame.

Let $\hat{\mathbf{S}} = \{\hat{S}_{f_k}^{p_k} : 0 \leq k \leq N_F - 1\}$ be the preamble that is detected by the receiver. This preamble detection procedure uses the following two properties of the transmitted preamble:

1. *The known order of the sequences*. Given the set of ZC sequences, $\{p_0, \ldots, p_{N_F-1}\}$, used in the preamble, $\hat{\mathbf{S}}$ must be found such that $f_0 < f_1 < \cdots < f_{N_F-1}$. This increases the number of possible preambles by allowing for different preambles to be constructed using the same set of ZC sequences, but with different subband orders.
2. *Location of the correlation peaks*. Multiple ZC sequences sent by the same transmitter as part of a single preamble will arrive at the receiver at approximately the same time. However, due to frequency-selective fading, the peaks may not be precisely aligned in time. To account for this, we use a threshold, ξ, to limit the range of acceptable separation between peaks—only sets of correlation peaks that are within ξ samples apart are considered as candidates for the preamble.

Algorithm 1 shows the pseudocode of the multipreamble detection. In lines 1-12, RODIN searches for the ZC sequence that is transmitted in each subband. Observe that we use **parallel-for** loops for this search step since in an FPGA implementation, all iterations of these **parallel-for** loops can be executed concurrently to reduce the search time. In lines 13-24, RODIN searches for a set of subbands $\{f_0, \ldots, f_{N_F-1}\}$ that contain the sequences $\{p_0, \ldots, p_{N_F-1}\}$ such that $f_0 < \cdots < f_{N_F-1}$ must hold. Note that this **for** loop cannot be parallelized because the result of each iteration depends on the result of the previous iteration.

4.4 Intersubband Interference

Observe that RODIN does not apply any filter to isolate each subband before conducting a search for a ZC sequence. This choice is made to avoid the additional delay that comes with a filtering step. However, there is now a possibility that sequences on different subbands interfere with each other during the correlation-based search. This possibility is present regardless of the type of sequence used, for example, Gold, ZC, Walsh-Hadamard, and so on. However, we argue that the possibility of intersubband collisions in our preamble design is very low.

A collision between two subbands can occur only if two or more different transmitters 1) select the same ZC sequence, 2) apply the same cyclic shift to the sequence, and 3) transmit at almost the same time. We posit that the probability of all three events occurring at even two noncolluding transmitters is very low. To gain some insight into this, first recall that in CSMA networks, the random backoff process undertaken by each transmitter minimizes the possibility of simultaneous transmissions. Even if simultaneous transmissions do occur, the set of ZC sequences can be made large enough to minimize the probability of collisions. For example, if we use ZC sequences of length 73, there are a total of $73 \times 73 = 5{,}329$ possible sequences that can be used by RODIN. The

TABLE 1
Time Required for Preambles Constructed with ZC of Length 37, 73, and 113 to Be Transmitted at 5-, 10-, and 20-MHz Bandwidths

		Preamble Length		
		37	73	113
BW (MHz)	5	$7.4\mu s$	$14.6\mu s$	$22.6\mu s$
	10	$3.7\mu s$	$7.3\mu s$	$11.3\mu s$
	20	$1.8\,us$	$3.65\mu s$	$5.56\mu s$

probability of two devices picking the same sequence is a mere $(1/5{,}329)^2 = 3.5 \times 10^{-8}$. Hence, intersubband interference does not affect the performance of I-FOP.

Algorithm 1: I-FOP detection.

Input : Set of ZC sequences $\mathbf{P} = \{p_0, \ldots, p_{N_F-1}\}$ RF sampling data stream, $\hat{y}[n]$, Correlation threshold, γ
Output: Occupied subbands $\mathbf{f} = \{f_0, \ldots, f_{N_F-1}\}$

1 **parallel-for** $k \in 0, \ldots, N-1$ **do**
2 /* Shift subband f_k to baseband */
3 $w_k[n] \leftarrow \hat{y}[n] \cdot e^{j2\pi f_k n/N}$;
4 **parallel-for** $l \in 0, \ldots, N_F - 1$ **do**
5 /* Correlate with p_l */
6 $\rho_{k,l}[n] \leftarrow (w_k \star p_l)[n]$;
7 $\lambda_{k,l} = \max_{0 \le m \le \xi} \rho_{k,l}[n-m]$;
8 **end-parallel-for**
9 /* Determine the ZC sequence on subband k */
10 $\sigma_k \leftarrow \arg\max_{0 \le l \le (N_F-1)} \lambda_{k,l}$;
11 $\eta_k \leftarrow \max_{0 \le l \le (N_F-1)} \lambda_{k,l}$;
12 **end-parallel-for**
13 $l \leftarrow 0$;
14 **for** $k \in 0, \ldots, N-1$ **do**
15 $f_l \leftarrow \infty$;
16 **if** $\sigma_k = p_l$ *and* $\eta_k > \gamma$ **then**
17 $f_l \leftarrow k$;
18 $l \leftarrow l + 1$;
19 **end**
20 **if** $l = N_F$ **then**
21 **return** $\mathbf{f} = \{f_0, \ldots, f_{N_F-1}\}$;
22 **end**
23 **end**
24 **return** $\mathbf{f} \leftarrow NULL$;

4.5 I-FOP Delay

The spectrum-shaping delay incurred by I-FOP depends on two parameters: the length of the chosen ZC sequence, and the bandwidth at which each sequence is transmitted. Table 1 shows the transmission time required for each sequence built from ZC codes of 37, 73, and 113 samples long at 5, 10, and 20 MHz. These subband bandwidths are suitable for use by 802.11 devices. The bandwidth of each transmitted sequence $S_{f_k}^{p_k}$ must be no larger than the bandwidth of each subband.

The delay at the receiver is due mainly to the processing time needed to find I-FOP. For every new sample, $\hat{y}[n]$, received by the detector in Algorithm 1, the **parallel-for** loops operate in constant $O(1)$ time while the search in lines 13-24 takes $O(N)$ time. With sufficient FPGA resources for full parallelism, the search can be completed in N clock cycles, or $(0.0225N)$ μs with a 40-MHz FPGA.

As an example, if we spectrally shape a 20-MHz 802.11n over a $B = 40$ MHz RF bandwidth using the 64-tap filter from Section 3.3 and a preamble based on a length-37 ZC sequence, the overall delay is $1.65 + 7.4 = 9.05$ μs. This is merely 3.8 percent of the transmission time of a 54-Mbps 802.11n frame. The delay incurred by I-FOP may exceed the SIFS delay of Wi-Fi COTS devices and trigger an ACK time-out at the transmitter. However, these ACK time-outs can be easily changed in software [1] and do not pose a hurdle to SDR-COTS integration. This local SIFS modification allows the attached COTS device to account for the extra delay from I-FOP; other non-RODIN Wi-Fi devices can operate normally without modifications.

4.6 Preamble Address Assignment

RODIN devices must assign an address to each flow in a distributed manner before spectrum agreement between devices is completed. Addresses to new flows are assigned using an *association frame*.

An association frame is a control frame sent between RODIN devices, and is not passed to the COTS device. Each association frame is spectrally shaped to occupy only the available subbands and is prepended with a preamble constructed using a fixed set of ZC sequences. This set of ZC sequences is the *association set* and is known to all RODIN devices. The association frame contains only the IDs of the ZC sequences and the order in which they will be used.

A RODIN receiver searches all subbands for the association set. Once this association set is found, RODIN recovers the association frame using the spectrum shaper from Section 3. It then decodes the frame to obtain the ZC sequence information that will be used for subsequent frames from the same flow. Once an address has been assigned, all transmissions belonging to the same flow, even if they originate from different RODIN devices (e.g., DATA and ACK frames), use the same preamble address.

Since the information carried in the association frame is small, the size of the frame is small, especially when compared with the total size of the flow. Hence, the overhead of address assignment is negligible.

4.7 Subband Selection

The transmitter selects the subbands by choosing the N_F subbands that have the lowest energy levels at the point of frame transmission. We make use of a Fast Fourier Transform (FFT)-based energy detector—we take the FFT of incoming samples and measure the magnitude of the energy in each subcarrier. On the 40-MHz FPGA, for example, a 128-bin FFT takes approximately 5 μs. Hence, energy values at any point in time are delayed by about 5 μs. This is acceptable because the channel state does not vary significantly over that short duration. Note that energy sensing delay decreases as the FFT length gets shorter.

On a faster and larger FPGA, we can also implement more advanced spectrum-scanning techniques, such as those based on the spectrum correlation function [13]. This will enable RODIN to not only detect the currently occupied subbands, but also determine the protocol occupying them and predict future usage patterns of the interferer.

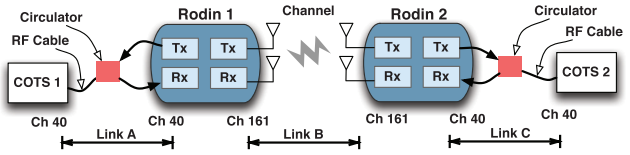

Fig. 7. Experimental setup. Each RODIN device is connected to a COTS device via a coaxial cable.

5 Spectrum Management

Algorithm 2 shows the pseudocode that defines the operation of the Spectrum Manager. RODIN is in the receive state until frames are detected from the COTS device. In this state, the RX spectrum-shaping filters are configured to span the occupied spectrum indicated by each received I-FOP.

Algorithm 2: Spectrum Manager.

```
while True do
    while No frame from COTS device detected do
        ŷ[n] ← next sample from RF frontend;
        if Preamble detected at ŷ[n] then
            Configure Rx Spectrum Shaper to span
            subbands of next frame;
        end
        Send ŷ[n] to Rx Spectrum Shaper;
        Send output of Rx Spectrum Shaper to COTS
        wireless device;
    end
    while Frame from COTS device detected do
        Configure filters in Tx Spectrum Shaper to
        appropriate subbands, if necessary;
        Configure Tx Preamble to tag occupied
        subbands;
        Transmit preamble from Tx Preamble;
        x[n] ← next sample from COTS device;
        Send x[n] to Tx Spectrum Shaper;
        Send output of Tx Spectrum Shaper to RF
        frontend;
    end
end
```

When a frame is transmitted by the COTS device, RODIN first configures the TX spectrum-shaping filters and TX I-FOP to span the transmit spectrum subbands. The preamble is then transmitted while the samples from the COTS device are filtered and modulated. The spectrally shaped samples are transmitted after I-FOP transmission is complete.

6 Evaluation: Spectrum Shaping

6.1 Experiment Setup

Fig. 7 illustrates the setup used for evaluating the performance of individual RODIN devices. Each RODIN spectrum shaper is implemented in Verilog/VHDL and runs on the FPGA of a WARP platform with four radios. Each radio is permanently set to either the Tx or Rx mode. One pair of Tx/Rx radios from each WARP device is connected to a *circulator* that is then connected to a COTS device. These connections are made using coaxial cables. A circulator routes passband signals between the COTS device and the two radios on the WARP—analog signals coming from the COTS device is sent only to the Rx radio on the WARP, while signals from the Tx radio on the WARP are routed only to the COTS device. Signals between the Rx and Tx radios are blocked by the circulator.

The circulator is used here so that RODIN can receive frames from the COTS device without the Tx-Rx switching delay that will otherwise be incurred by the radio hardware if only one radio is connected to the COTS device. The other two Tx/Rx radios on each WARP device are connected directly to antennae. The two RODIN devices are placed approximately 2-m apart. We have successfully used Ralink 802.11a Wi-Fi card for COTS 1 and 2. However, to achieve finer-grained control of the transmitted signal for experimental purposes, we use WARP for COTS 1 and 2 for the rest of the experiments.

We send uncoded OFDM frames with a bandwidth of 10 MHz between the two COTS devices. The spectrum of the OFDM frames can be shaped to span any 10 MHz of spectrum within the 20-MHz maximum bandwidth supported by each radio. For all experiments in this section, we split the 10-MHz OFDM frame into two subbands of 5 MHz each. These subbands are transmitted with a 10-MHz separation between them.

Each RODIN device detects transmissions from its attached COTS device by checking the RSSI of the Rx radio that is directly connected to the circulator. If the RSSI exceeds a predefined threshold, the COTS device is assumed to be transmitting. This can be done easily as the SNR of transmissions over the coaxial cable is high. At all other times, the Tx radio continuously transmits received signals to the COTS device for receiver processing. This maintains the capability of the COTS device to overhear transmissions from other devices that share the same discontiguous spectrum.

We use two metrics to measure the performance of the spectrum shaper: *error vector magnitude* (EVM), which is shown as a percentage, and *bit error rate* (BER), which is the fraction of bits received in error.

6.2 Spectrum Shaping Results

6.2.1 Without Interference

We transmit 2,000 OFDM frames using QPSK symbols from COTS 1 to COTS 2 using the setup in Fig. 7, and measure the mean EVM of the frames between each pair of directly connected devices. This experiment is conducted twice, once with and once without spectrum shaping. Fig. 8 shows the CDF of measured EVM. One important conclusion from this result is: *Spectrum shaping does not distort the signal.* The CDF of the EVM over each OFDM frame is identical with and without spectrum shaping of the transmitted OFDM frame. Hence, real-time spectrum shaping can be implemented in the FPGA without any loss of signal quality.

Direct manipulation of a signal from a COTS device with an attached RODIN platform does introduce some distortion into the signal. The median EVM of frames sent over Link A of Fig. 7 is 7 percent, while median EVM of the frame that is spectrally shaped and sent over Link B is 9 percent. Finally, the transmission over Link C to COTS 2 increases the median EVM to 11 percent. (An EVM of 11 percent is small enough not to increase BER; BER of all frames transmitted

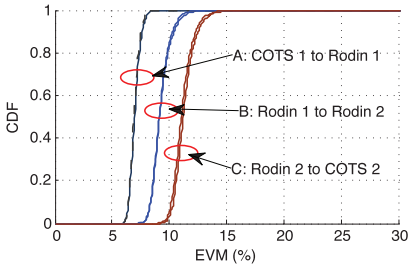

Fig. 8. EVM of symbols in an OFDM frame with and without spectrum shaping. No interference.

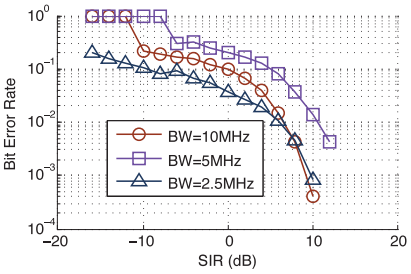

Fig. 10. BER of OFDM frames measured at COTS 2 without shaping. No errors are encountered when spectrum shaping is used.

in Fig. 8 is zero.) These additional distortions are introduced during 1) up and down signal modulation by the AD/DA converters at both COTS devices and the radios on the WARP, and 2) time and frequency offsets between the COTS device and its attached WARP. Both of these sources of distortion can be eliminated by tighter integration between RODIN and the COTS device: distortion due to up/down converters can be reduced by passing the baseband signal directly between RODIN and the COTS device; distortion due to time and frequency offsets can be mitigated by synchronizing RODIN with the clock used by the COTS device.

6.2.2 With Interference

We transmit an interfering signal using another WARP device. The transmission power of this signal is varied to achieve a range of signal-to-interference ratios (SIR). At each interference power level, we transmit the interference at three different bandwidths—2.5, 5, and 10 MHz. Fig. 9 shows the EVM of a 10-MHz OFDM frame sent from COTS 1 to COTS 2 that experiences interference with bandwidth 2.5, 5, and 10 MHz. This experiment is conducted over a range of SIR levels, with and without RODIN spectrum shaping.

We first consider the performance of spectrum shaping. The mean EVM of the OFDM transmission when SIR is greater than -2 dB is 11 percent. This is equivalent to a spectrum-shaped OFDM transmission in the absence of interference, as shown in Fig. 8. At SIR levels lower than -2 dB, the impact of interference on the OFDM transmission depends heavily on the interference bandwidth—interference with a 10-MHz bandwidth increases the EVM to almost 40 percent while it remains at 11 percent when the bandwidth is 2.5 MHz. This variation is due to the fact that filters used to generate the interference signal are not ideal. Hence, some energy leakage occurs at the edges of the filter. Although the two subbands of the spectrum-shaped OFDM frame are separated by 10 MHz, they are still affected by the leaked interference energy. With a 10-MHz interference bandwidth, the leakage energy is sufficient to distort the spectrum-shaped transmission. At 2.5 MHz, the bandwidth of the interference is small enough that power leakage due to imperfect filters does not have a noticeable impact on the main OFDM transmission.

Without spectrum shaping, the narrowband interference has a significant impact on the OFDM transmission. For a given interference power, the smaller the interference bandwidth, the greater the interference power per subcarrier. The effect of this is seen from the fact that the distortion of the OFDM frames from the 5-MHz interference is greater than that from the 10-MHz frames—the increased interference power on fewer subcarriers is high enough to make up for the reduction in the number of subcarriers that encounter interference. When the interference bandwidth is at 2.5 MHz, the small number of subcarriers affected allows the EVM to fall below that when a 10-MHz interference is used.

This behavior is also evident when we consider the BER of the OFDM frames, as shown in Fig. 10. With spectrum shaping, the primary OFDM frames are sent on frequency bands that are not occupied by the interfering signal. The BER is, thus, zero for spectrum-shaped OFDM frames. Without spectrum shaping, the OFDM frame has a BER of 1.0 when it encounters a 10- or 5-MHz interference at SIR below -12 dB. The BER of the OFDM frame with a 2.5-MHz interference is expectedly lower than that at interference bandwidths of 5 and 10 MHz, but still stands at a high 1 percent at 8-dB SIR.

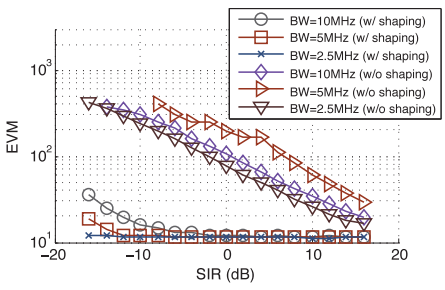

Fig. 9. Mean EVM of OFDM frames measured at COTS 2 under different SIR levels.

7 Evaluation: I-FOP

In this section, we study the performance of I-FOP with two experiments: 1) under channels with varying SNR and SIR levels, and 2) in realistic multidevice contention scenarios.

7.1 SNR/SIR Performance

7.1.1 Experiment Setup

We evaluate I-FOP using five WARP devices placed at various locations around an office. Since the objective of this experiment is to evaluate the feasibility and performance of our preamble design, we run experiments using WARPLab+MATLAB instead of an FPGA-based WARP implementation. The results obtained using WARPLab and an FPGA implementation will be identical.

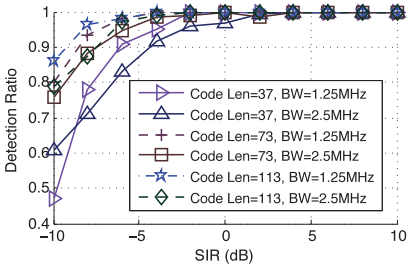

Fig. 11. Preamble detection rate of three codeword lengths over $N = 8$ subbands on a 20-MHz channel in the presence of interfering preambles. Each preamble is transmitted at 2.5 and 1.25 MHz.

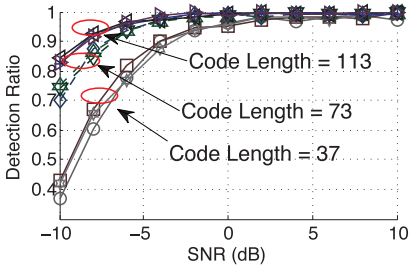

Fig. 12. Preamble detection rate of three different codeword lengths over $N = 8$ subbands on a 20-MHz channel. Each preamble is transmitted under 0-, 12-, and 20-dB SNR.

The performance of I-FOP is evaluated under SIRs ranging from -10 to 10dB. This interference consists of different I-FOPs that overlap with the transmission of the primary I-FOP. The result for each SIR is the mean of 2,000 preamble transmissions. In each transmission, we select a random receiver, transmitter, and interferer from five WARP devices. We use a 20-MHz channel with $N = 8$ subbands (each subband is, thus, 2.5-MHz wide). Three different preamble lengths are evaluated: 37, 73, and 113 samples. For every preamble, we randomly select $N_F = 4$ subbands and transmit a different ZC sequence on each one. All ZC sequences are transmitted at the same bandwidth.

The receiver searches for the known ZC sequences that belong to the primary preamble transmission using the procedure shown in Algorithm 1. If the set of ZC sequences is found in the specified order, the preamble is considered to be detected. Otherwise, a missed detection is recorded.

We also evaluate the performance of the preamble under varying SNR levels. However, due to the difficulty of accurately controlling the noise level in the channel, SNR evaluations are conducted using a simulated 802.11 channel.

Fig. 11 shows the detection probability of preambles with three different lengths, in the presence of overlapping interfering preambles. We run two experiments, with each one conducted over a range of SIR values. In the first experiment, each ZC sequence of every preamble (both the intended and interfering preambles) is sent at 2.5 MHz (equal to the bandwidth of the subband); in the second experiment, each ZC sequence is sent at 1.25 MHz, half the subband bandwidth. Interfering preambles are transmitted with a random time offset with respect to the noninterfering ones.

7.1.2 SIR Performance

Observe that for preambles with the same length, the detection accuracy is greater as the bandwidth of each ZC sequence is reduced for two reasons. First, as the sampling rate of WARP is constant, the longer correlation period that results from a lower bandwidth ZC sequence gives a higher correlation peak magnitude when a match is found. Second, when ZC sequences are transmitted at 1.25 MHz, there is a guard band between sequences on adjacent subbands. This reduces the intersubband interference that arises due to energy leakage from adjacent subbands. No guard bands are present when the ZC sequences are sent at 2.5 MHz.

Also, observe that the detection ratio increases with increasing ZC sequence length. This is because the peak autocorrelation magnitude is proportional to the sequence length L, while the cross-correlation magnitude of $1/\sqrt{L}$ actually *decreases* with increasing sequence length. These two effects cause the SNR of the correlation peak to increase with increasing ZC sequence length.

7.1.3 SNR Performance

The accuracy of the preamble detector is similar over a wide range of SNR values, as shown in Fig. 12. For each ZC sequence length, we transmit the preamble at 0-, 12-, and 20-dB SNR. Observe that accuracy is largely unaffected by the SNR level on the channel and is primarily dependent on the interference power.

In our experiments, the probability of detecting an I-FOP preamble when no I-FOP is present (false positive) is zero. False positives may occur due to ZC sequence collisions or more complicated channel fading scenarios. We can mitigate the effects of fading by using Rake correlators to search for the ZC sequences. However, false positives have limited impact on the operation of RODIN as the falsely received frame/signal are simply discarded by the COTS device.

7.2 Contention Performance

7.2.1 Experiment Setup

We use 16 WARP devices to demonstrate the accuracy of I-FOP under realistic channel-contention scenarios. For each experimental run, we use 16 devices that are nonuniformly distributed throughout an office. We randomly select four transmitters and four receivers, each using a 20-MHz channel with $N = 8$ subbands. Each Tx-Rx pair uses a nonoverlapping set of $N_F = 2$ subbands for communications. The four Tx-Rx pairs do not transmit simultaneously. Instead, a randomly selected jitter between 5 and 100 μs is injected into each Tx-Rx pair in every experimental run. Note that this *injected* jitter is not equal to the *actual* transmit jitter due to the difficulty of synchronizing WARP devices perfectly. The actual jitter can differ from the injected jitter by up to 2 μs. We will show the aggregate results of 1,000 such runs.

We demonstrate the accuracy of I-FOP in two ways. First, at each receiver, we show the window of ξ samples within which the correlation peaks of the ZC sequences from the same transmitter are detected. The smaller the necessary ξ samples, the lower the rate of missed detections. Second, we show the accuracy at which each receiver can differentiate between preambles from different transmitters. To do this, we search for all ZC sequences at every receiver, and compare the maximum separation between the received

position of ZC sequences from different nodes to the injected jitter used in the transmission. We refer to this maximum separation gap as the *position error*.

7.2.2 Correlation Peaks from the Same Transmitter

Fig. 14 shows the CDF of the separation between correlation peak of ZC sequences from the same transmitter. In 1,000 experiments, over 99 percent of the correlation peaks of ZC sequences coming from the same transmitter are found within five samples ($0.125\ \mu$s) of each other. Furthermore, almost 100 percent of peaks were seen within 20 samples ($0.5\ \mu$s) of each other. Hence, by setting $\xi = 20$, we can use the location of correlation peaks to accurately detect almost all preambles.

7.2.3 Correlation Peaks from Different Transmitters

Fig. 15 shows the CDF of the position error of ZC sequences from different transmitters. Observe that 99 percent of the ZC sequences are detected within 100 samples ($2.5\ \mu$s) of their transmission time. Note that this position error includes the possible difference between the actual and injected jitter from imperfect synchronization. However, this still provides strong evidence that I-FOP can successfully discriminate between transmitters if transmission times are separated by at least $2.5\ \mu$s.

8 Evaluation: RODIN

We evaluate the performance of RODIN using simulations over detailed channel measurements from [29]. These channel measurements show the usage behavior of devices that operate on three separate bands. During periods when the channel RSSI is low, primary user activity is absent and spectrum agile devices can transmit opportunistically. Our objective is to show the efficacy of per-frame spectrum shaping in using these short-term transmission opportunities.

8.1 Simulation Setup

8.1.1 Trace Data

Each channel measurement of [29] spans a 1.6-GHz bandwidth that is centered at three different frequencies 770, 2,250, and 5,250 MHz, so they cover the 2.4- and 5-GHz ISM bands used by Wi-Fi devices. Measurements were taken over several days at three different locations: for brevity, we only show results using the data set measured at rooftop of a school. Each sweep over the entire 1.6-GHz bandwidth takes about 1.8 s and captures 8,192 samples, with each sample spanning 200 kHz. Although the measurement data do not capture channel usage patterns shorter than 1.8 s, channel statistics have been shown to remain unchanged at shorter time scales [15]. This strongly suggests that we can expect such statistics to be present at sufficiently small time scales to make RODIN useful. Hence, our analysis using this data is still applicable even when considering finer-grained channel usage patterns.

8.1.2 Device Models

We model three different types of wireless devices in our simulations; two that support spectrum shaping and one that does not. The maximum RF bandwidth of each device is 20 MHz. The bandwidth of transmitted signal is 10 MHz, with the remaining 10-MHz bandwidth used for spectrum reallocation. There are three models as follows:

1. RODIN. This model uses per-frame spectrum shaping and the multisubband preamble. We experiment with two different SDR RF bandwidths of 20 and 40 MHz; for each RF bandwidth, we use subband bandwidths of 1 and 2 MHz. The bandwidth of the COTS signal is half of the SDR bandwidth, with the other half of the SDR bandwidth used for spectrum reallocation. For example, a RODIN device with a SDR and COTS bandwidth of 20 and 10 MHz, respectively, and a subband bandwidth of 2 MHz will require $N_F = 5$ subbands to span the COTS bandwidth and $N = 2N_F$ subbands to span the SDR bandwidth. At the beginning of each measurement slot (1.8 s), RODIN measures the RSSI of all subbands and selects the N_F subbands with the lowest RSSI. This is equivalent to selecting the set of N_F subbands with the lowest interference powers. If all subbands have RSSIs lower than a predefined threshold, RODIN transmits a frame over those time slots. RODIN can carry out this measure-shape-transmit process within a single time slot due to its per-frame spectrum agreement and shaping capability. The performance of RODIN is modeled based on the I-FOP detection probability measured in the previous section.
2. *COTS-Spec.* This model can bond multiple subbands for a single transmission, but cannot change the bonding on a per-frame basis. The bandwidth configuration used in COTS-Spec is identical to that of the RODIN model. At the beginning of a time slot (1.8 s), it selects the N_F subbands with the lowest RSSI as before. However, these selected subbands are used only in the *next* time slot. The set of subbands used for the current transmission is selected in the previous time slot. This represents the delay required by a COTS device to switch to a different set of subbands. Note that this is an optimistic model because 1) we do not consider the additional overhead required for spectrum agreement, and 2) we assume that COTS-Spec can continue to transmit in the current time slot even as it is changing its set of bonded subbands.
3. *COTS-Mono.* In this model, the COTS device makes use of the middle 10- or 20-MHz bandwidth of the channel (depending on the bandwidth of the COTS device) for transmitting a frame, but no spectrum shaping is used. This represents a typical 802.11-type device that uses monolithic spectrum blocks for transmission.
4. *Oracle.* This is the RODIN model with a subband bandwidth of 200 kHz (the smallest allowable bandwidth with the trace data). This models the performance of RODIN without any limitations on the bandwidth and number of its subband filters.

8.1.3 Channel Model

We are interested in finding the number of time slots during which each of these models can find a transmission opportunity. We evaluate the performance of the four models using two channel bandwidths of 20 and 40 MHz.

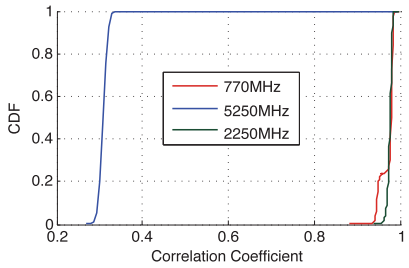

Fig. 13. CDF of the correlation of the RSSI seen across all measurement slots over time.

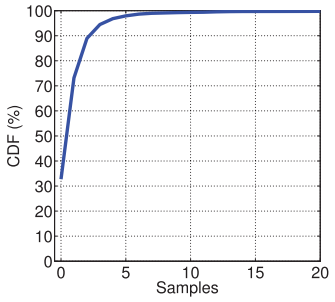

Fig. 14. Difference between correlation peaks of ZC sequences from the same transmitter.

The RF bandwidth of the SDR is set to 20 and 40 MHz, respectively. To evaluate the performance of each model, we partition the frequency slots each of the three traces into nonoverlapping 20- or 40-MHz channels and simulate the operation of each model on all the channels. The threshold levels that we use for 770-, 2,250-, and 5,250-MHz trace sets are -100, -90, and -90 dBm, respectively. These are chosen to be similar to the 802.22 standard for 770-MHz data set and the 802.11 standard for the others. Any 200-kHz time-frequency slot with an RSSI that exceeds this threshold is assumed to be occupied by a primary transmitter. A subband is considered to be available at a particular time if and only if all frequency slots at that time have RSSIs lower than the threshold. We assume that there is only a single transmitter-receiver pair in each channel as it is sufficient to capture the behavior of the device models under a wide range of channel conditions. We leave the study of RODIN-to-RODIN interference to future work.

8.2 Simulation Results

8.2.1 Channel Characteristics

The gain from per-frame spectrum shaping depends on the temporal variability—the more frequently the interference

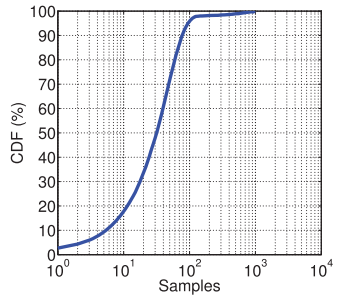

Fig. 15. Position error of ZC sequences from different transmitters.

level on the channel changes, the greater the need for fast spectrum shaping. Fig. 13 shows the correlation coefficient of the RSSI on each measurement slot over time, for each trace set. Channels within the 5,250-MHz data set experience high temporal variability and have a median correlation coefficient of about 0.3. On the other hand, channels within the 770- and 2,250-MHz data sets experience minimal temporal variability, as seen by the high correlation coefficients. We expect the gain from per-frame spectrum shaping to, thus, be greater in the 5,250-MHz channels than in channels at other frequencies.

8.2.2 Transmission Time Slots

Fig. 16 shows the proportion of time slots in each channel in which the different devices can find transmission opportunities. Note that the channels are labeled in increasing order of their center frequencies. In the 5,250-MHz trace set, as shown in Fig. 16a, the high temporal variability of the channel means that subbands found to be available for transmission in one time slot are unlikely to still be available in the next time slot. Hence, COTS-Spec with 1-MHz subbands can only transmit in up to 15 percent time slots. COTS-Spec with 2-MHz subbands fails to find any transmission slots. A surprising result is that the performance of COTS-Mono is almost identical to that of COTS-Spec with 1-MHz subbands. This shows that under highly varying channels, slow channel adaptation with narrow subbands performs almost identically to no spectrum adaptation; while slow channel adaptation with wider subbands fails to find any transmission opportunities.

The per-frame spectrum shaping of RODIN enables it to transmit on a significantly larger proportion of the time slots—up until 95 percent of the time slots in channel 81. Furthermore, we note that time slot utilization is increased when we use smaller subband bandwidths—RODIN using

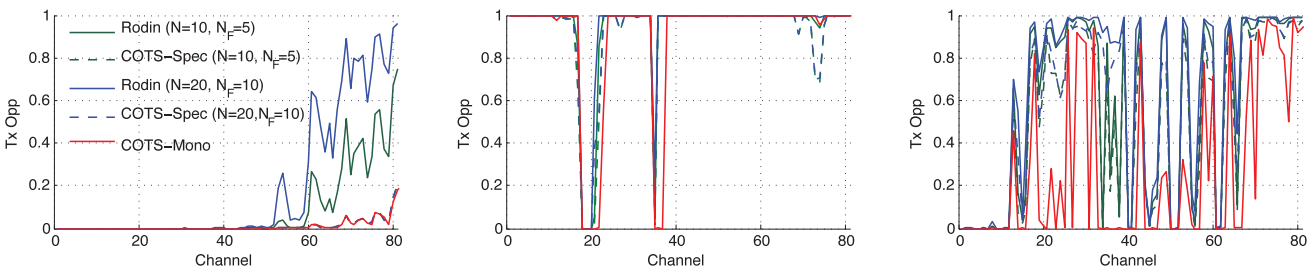

(a) 5250MHz. (b) 2250MHz. (c) 770MHz.

Fig. 16. Proportion of time slots that each of the devices, RODIN, COTS-Spec, and COTS-Mono, can transmit in.

1-MHz subbands ($N = 20$, $N_F = 10$) can outperform the same device using 2-MHz subbands ($N = 10$, $N_F = 5$) by more than 50 percent in some channels. Note that channels 1-50 in the 5,250-MHz data set fall into spectrum that is completely occupied by interferers. Hence, no slots can be found by any devices.

The performance of COTS-Spec improves under the low temporal variability of the 770- and 2,250-MHz trace sets. Fig. 16b shows that the fraction of time slots used by COTS-Spec is almost equal to that used by RODIN for transmissions. However, in Fig. 16c, we see that even in channels with high correlation coefficients, RODIN still finds more transmission opportunities than COTS-Spec at the same subband bandwidth. This is seen between channels 20 and 30. COTS-Mono performs poorly even on channels with low temporal variation, as shown in both Figs. 16b and 16c. Spectrum shaping is still necessary here as the low temporal channel variability does not imply the widespread availability of high bandwidth channels.

9 Discussion

9.1 How Does RODIN Affect Carrier Sensing?

RODIN departs from the typical carrier sensing policy and enables COTS devices to transmit even if one or more subbands are occupied. We assume that the COTS devices use N_F out of N total subbands. RODIN continuously monitors all subbands and sends the channel state from N_F subbands with the lowest channel noise to the COTS for carrier sensing. More precisely, RODIN follows the following two steps:

Step 1. During periods without COTS transmission, RODIN maintains an exponentially weighted moving average (EWMA) of the noise energy in all the N subbands. For each subband, this filtering operation can be expressed as $e_{\text{EWMA}} = (1-\alpha)e_{\text{EWMA}} + \alpha e$, where e_{EWMA} and e are the EWMA-filtered and the most recent noise energy values from the subband, and α is the EWMA weight. To determine the latency of this filtering operation, first note that α and $1-\alpha$ are precomputed constants. The two multiplication operations occur in parallel and require one clock cycle (or 0.025 μs in a 40-MHz FPGA). The addition operation also requires one clock cycle. Assuming that each measured noise energy value e requires 5 μs (from Section 4.7), monitoring the energy of each subband incurs a latency of merely 5.05 μs. Note that all channels are monitored in parallel.

Step 2. RODIN then selects the N_F subbands with the lowest noise energy levels. The sum of the noise energy from these N_F subband is sent to the COTS devices for carrier sensing. This step is identical to the subband selection step used by I-FOP in Section 4.7.

9.2 How Does RODIN Affect Receiver Equalization?

RODIN can partition a narrowband COTS signal into subbands that are placed spectrally far apart (e.g., on the ISM and 700-MHz bands). Hence, the fading characteristics encountered by different subbands can be very different and the COTS PHY may not have enough pilot tones to equalize the received signal.

The impact of RODIN spectrum shaping on multicarrier (e.g., OFDM) COTS PHYs is limited as the receiver CSI is measured on a per-subcarrier basis. Hence, the COTS device can still compensate for the channel distortion on each subcarrier. The pilot tones can then be used to track channel variations after the primary synchronization step is complete.

To further mitigate the effects of heterogeneous channel fading characteristics, RODIN can include additional RODIN-specific CSI training sequences in each transmission. The RODIN receiver will equalize each subband separately before forwarding the recombined received signal to the COTS device. This will come at the price of greater latency in the RODIN platform, along with greater FPGA resource requirements.

9.3 Are the ADCs/Mixers in RODIN Sensitive to Strong Interference?

Strong interference over the RF cable between the COTS and the SDR will degrade the signal quality as RODIN does not implement any equalization techniques to correct distortions in the COTS transmission over the RF cable. In our RODIN prototype, the RF interface that is directly connected to the COTS device should operate on a channel with minimal noise and interference. Our experiments have shown that in the absence of external interference, any equalization produces limited benefit over the already low signal distortion of the RF cable. This is a limitation of our experimental setup but is not a shortcoming of the RODIN architecture as proper shielding on this well-defined COTS-SDR communication channel can easily mitigate the impact of external interference.

10 Related Work

10.1 Spectrum Agility

WhiteFi [3] is a variable-bandwidth 802.11-based prototype that provides protocols that govern channel-switch triggers, channel probing, and selection in whitespaces. This idea of variable-bandwidth communications is also used by FLUID [20] in enterprise networks. Jello [30] extends this variable bandwidth idea to support noncontiguous channel bonding in challenging networks. TIMO [10] adopts a different approach to handling interference on MIMO channels, treating interference as a single MIMO streams while simultaneously transmitting frames on the remaining MIMO streams. SVL [25] and Picasso [14] are both spectrum-shaping layers for general wireless devices. However, these solutions require tight integration with the COTS device's PHY and are not fast enough to support per-frame shaping. The new IEEE 802.11ac standard draft also specifies *noncontiguous* $80 + 80$ *MHz* channel bonding as an optional feature [2], but does not support per-frame shaping. SWIFT [19] supports transmissions over noncontiguous bands while avoiding interference from narrowband devices. However, it differs from RODIN as it does not support per-frame spectrum shaping and agreement. Furthermore, it is not compatible with any available COTS devices and networks.

10.2 Spectrum Agreement

SIFTs [3], part of WhiteFi, is a single-channel bandwidth-independent signal detection algorithm used for determining the transmit bandwidth of an AP. FICA [24] uses binary

amplitude modulation on multiple OFDM subcarriers, together with tight time synchronization, to enable each device to contend for different spectrum bands. Preamble detection on NC-OFDM networks [9] is useful for communications over disjoint spectral bands, but a separate mechanism must first be used to agree on the spectrum bands. Other typical uses for spectrum agreement include control channels [31] and backup channel lists [23].

11 Conclusion

We presented RODIN, a DSA extension platform that supports 1) direct connection to a COTS device, 2) fast FPGA-based spectrum shaping, and 3) I-FOP for fast and accurate spectrum agreement. A complete spectrum agreement and shaping operation can be carried out in about 10 μs, which adds only approximately 3.8 percent overhead to an 802.11n frame. We evaluated spectrum shaping and I-FOP using both simulations and real-world experiments, and demonstrated their efficacy even under low SIR levels.

Acknowledgments

The work reported in this paper was supported in part by the US National Science Foundation under Grants CNS-1160775 and CNS-1317411.

References

[1] "Linux ath9k Driver," http://wireless.kernel.org/en/users/Drivers/ath9k, 2013.
[2] *Proposed TGac Draft Amendment (Draft 3.1) for IEEE 802.11 Wireless LANs,* IEEE, Aug. 2012.
[3] P. Bahl, R. Chandra, T. Moscibroda, R. Murty, and M. Welsh, "White Space Networking with Wi-Fi Like Connectivity," *Proc. ACM SIGCOMM Conf. Data Comm.,* 2009.
[4] V. Brik, S. Banerjee, M. Gruteser, and S. Oh, "Wireless Device Identification with Radiometric Signatures," *Proc. ACM MobiCom,* 2008.
[5] R. Chandra, R. Mahajan, T. Moscibroda, R. Raghavendra, and P. Bahl, "A Case for Adapting Channel Width in Wireless Networks," *Proc. ACM SIGCOMM Conf. Data Comm.,* 2008.
[6] C.-T. Chou, N.S. Shankar, H. Kim, and K.G. Shin, "What and How Much to Gain by Spectrum Agility?" *IEEE J. Selected Areas in Comm.,* vol. 25, no. 3, pp. 576-588, Apr. 2007.
[7] D. Chu, "Polyphase Codes with Good Periodic Correlation Properties," *IEEE Trans. Information Theory,* vol. 18, no. 4, pp. 531-532, July 1972.
[8] L. Deek, E. Garcia-Villegas, E. Belding, S.-J. Lee, and K. Almeroth, "The Impact of Channel Bonding on 802.11n Network Management," *Proc. Seventh Conf. Emerging Networking EXperiments and Technologies (CoNEXT),* 2011.
[9] A. Dutta, D. Saha, D. Grunwald, and D. Sicker, "Practical Implementation of Blind Synchronization in NC-OFDM Based Cognitive Radio Networks," *Proc. ACM Workshop Cognitive Radio Networks (CoRoNet),* 2010.
[10] S. Gollakota, F. Adib, and D. Katabi, "Clearing the RF Smog: Making 802.11 Robust to Cross-Technology Interference," *Proc. ACM SIGCOMM Conf.,* 2011.
[11] R. Gummadi, D. Wetherall, and B. Greenstein, "Understanding and Mitigating the Impact of RF Interference on 802.11 Networks," *Proc. ACM Conf. Applications, Technologies, Architectures, and Protocols for Computer Comm. (SIGCOMM '07),* 2007.
[12] M. Heusse and F. Rousseau, "Performance Anomaly of 802.11b," *Proc. IEEE INFOCOM,* 2003.
[13] S. Hong and S. Katti, "DOF : A Local Wireless Information Plane," *Proc. ACM SIGCOMM Conf.,* 2011.
[14] S. Hong, J. Mehlman, and S. Katti, "Picasso: Flexible RF and Spectrum Slicing," *Proc. ACM SIGCOMM Conf. Applications, Technologies, Architectures, and Protocols for Computer Comm. (SIGCOMM '12),* 2012.
[15] V. Kone, L. Yang, X. Yang, B.Y. Zhao, and H. Zheng, "On the Feasibility of Effective Opportunistic Spectrum Access," *Proc. 10th ACM SIGCOMM Conf. Internet Measurement (IMC '10),* 2010.
[16] S. Lakshmanan, J. Lee, R. Etkin, S.-J. Lee, and R. Sivakumar, "Realizing High Performance Multi-Radio 802.11n Wireless Networks," *Proc. IEEE Eighth Ann. Comm. Soc. Conf. Sensor, Mesh and Ad Hoc Comm. and Networks (SECON),* 2011.
[17] T. Lin and Y. Tseng, "Collision Analysis for a Multi-Bluetooth Picocells Environment," *IEEE Comm. Letters,* vol. 7, no. 10, pp. 475-477, Oct. 2003.
[18] M. Loiacono, J. Rosca, and W. Trappe, "The Snowball Effect: Detailing Performance Anomalies of 802.11 Rate Adaptation," *Proc. IEEE GlobeCom,* 2007.
[19] H. Rahul, N. Kushman, D. Katabi, C. Sodini, and F. Edalat, "Learning to Share: Narrowband-Friendly Wideband Networks," *ACM SIGCOMM Computer Comm. Rev.,* vol. 38, no. 4, pp. 147-158, 2008.
[20] S. Rayanchu, V. Shrivastava, S. Banerjee, and R. Chandra, "FLUID: Improving Throughputs in Enterprise Wireless LANs through Flexible Channelization," *Proc. ACM MobiCom,* 2011.
[21] I. Selesnick, M. Lang, and C. Burrus, "Constrained Least Square Design of FIR Filters without Specified Transition Bands," *IEEE Trans. Signal Processing,* vol. 44, no. 8, pp. 1879-1892, Aug. 1996.
[22] V. Shrivastava, S. Rayanchu, J. Yoon, and S. Banerjee, "802.11n under the Microscope," *Proc. Eighth ACM SIGCOMM Conf. Internet Measurement (IMC),* 2008.
[23] J. So and N. Vaidya, "Multi-Channel MAC for Ad Hoc Networks: Handling Multi-Channel Hidden Terminals Using a Single Transceiver," *Proc. ACM MobiCom,* 2004.
[24] K. Tan, J. Fang, Y. Zhang, S. Chen, L. Shi, and J. Zhang, "Fine-Grained Channel Access in Wireless LAN," *Proc. ACM SIGCOMM Conf.,* 2010.
[25] K. Tan, H. Shen, J. Zhang, and Y. Zhang, "Enable Flexible Spectrum Access with Spectrum Virtualization," *Proc. IEEE Int'l Symp. Dynamic Spectrum Access Networks (DySpan),* 2012.
[26] K. Tan, J. Zhang, J. Fang, H. Liu, Y. Ye, S. Wang, Y. Zhang, H. Wu, W. Wang, and G.M. Voelker, "Sora: High performance Software Radio Using General Purpose Multi-Core," *Proc. Sixth USENIX Symp. Networked Systems Design and Implementation (NSDI),* 2009.
[27] Ettus Research, "Introducing the New USRP," http://www.ettus.com, 2013.
[28] Mango Comm., "Wireless Open-Access Research Platform (WARP)," http://mangocomm.com, 2013.
[29] M. Wellens and P. Mähönen, "Lessons Learned from an Extensive Spectrum Occupancy Measurement Campaign and a Stochastic Duty Cycle Model," *Mobile Networks and Applications,* vol. 15, pp. 461-474, 2010.
[30] L. Yang, W. Hou, L. Cao, B. Zhao, and H. Zheng, "Supporting Demanding Wireless Applications with Frequency-Agile Radios," *Proc. Seventh USENIX Conf. Networked Systems Design and Implementation (NSDI),* 2010.
[31] Y. Yuan, P. Bahl, R. Chandra, and P. Chou, "KNOWS: Kognitiv Networking over White Spaces," *Proc. IEEE Second Int'l Symp. New Frontiers in Dynamic Spectrum Access Networks (DySPAN),* 2007.
[32] X. Zhang and K.G. Shin, "Adaptive Subcarrier Nulling: Enabling Partial Spectrum Sharing in Wireless LANs," *Proc. IEEE 19th Ann. Int'l Conf. Network Protocols (ICNP),* 2011.

Eugene Chai received the BS degree in 2006 from the National University of Singapore and the MSE degree in 2009 from the University of Michigan, Ann Arbor. He is working toward the PhD degree in the Computer Science and Engineering Department at the University of Michigan, under the guidance of Professor Kang G. Shin. His research interests lie in the design and implementation of next-generation software-defined wireless infrastructure networks. He is a student member of the IEEE.

Kang G. Shin is the Kevin & Nancy O'Connor professor of computer science in the Department of Electrical Engineering and Computer Science at The University of Michigan, Ann Arbor. His current research focuses on QoS-sensitive computing and networking as well as on embedded real-time and cyber-physical systems. He has supervised the completion of 74 PhDs and authored/coauthored more than 800 technical articles (more than 300 of these are in archival journals), a textbook, and more than 20 patents or invention disclosures. He has received numerous awards, including Best Paper Awards from the 2011 ACM International Conference on Mobile Computing and Networking (MobiCom '11), the 2011 IEEE International Conference on Autonomic Computing, and the 2010 and 2000 USENIX Annual Technical Conferences, as well as the 2003 IEEE Communications Society William R. Bennett Prize Paper Award and the 1987 Outstanding *IEEE Transactions of Automatic Control* Paper Award. He has also received several institutional awards, including the Research Excellence Award in 1989, Outstanding Achievement Award in 1999, Distinguished Faculty Achievement Award in 2001, and Stephen Attwood Award in 2004 from the University of Michigan (the highest honor bestowed to Michigan Engineering faculty); a Distinguished Alumni Award from the College of Engineering, Seoul National University in 2002; the 2003 IEEE RTC Technical Achievement Award; and the 2006 Ho-Am Prize in Engineering (the highest honor bestowed to Korean-origin engineers). He is a Life Fellow of the IEEE.

Jeongkeun Lee received the PhD degree in computer science from Seoul National University in 2007. He is a senior researcher at Hewlett-Packard (HP), working on various networking projects covering cloud, wireless, and mobile. He received two ACM MobiCom demo awards in 2007 and the HP CEO Innovation Award in 2010. His recent interest is on capturing applications' needs and enabling application-aware networking in cloud and wireless SDN. He is a member of the IEEE.

Sung-Ju Lee received the PhD degree in computer science from University of California, Los Angeles in 2000. He is a principal member of the technical staff at the office of the CTO of Narus, Inc. Before joining Narus, he was a principal research scientist and a distinguished mobility architect at Hewlett-Packard (HP). He has published 100 technical papers in peer-reviewed journals and conferences. His papers are well cited, with his publications receiving a total of nearly 9,000 citations. He currently holds 18 US patents and more than 40 pending patents. He received the HP CEO Innovation Award in 2010. He is a cofounder and a steering committee member of IEEE SECON. He is a fellow of the IEEE and an ACM distinguished scientist.

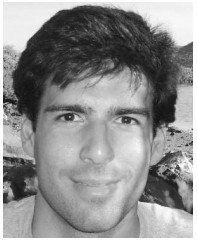

Raúl H. Etkin received the BS degree in electrical engineering (with honors) from the University of Buenos Aires, Argentina, in 1998, and the MS and PhD degrees in electrical engineering from the University of California at Berkeley in 2003 and 2006, respectively. He is a senior research engineer at Samsung Information Systems America, San Jose, California. From 2006-2013, he was a research scientist at Hewlett-Packard, where he worked on various problems in wireless communications and information theory. During the summers of 2002 and 2003, he was in the Corporate R&D Department at Qualcomm, Inc. He is a coinventor on several US patents. His current research interests include multiuser information theory, wireless communications, and spectrum sharing. He received the Gold Medal Award from the University of Buenos Aires, Argentina, the Best Engineers Award from the Argentine National Engineering Academy in 1999, and a Fulbright Fellowship in 2000. From 2000 to 2002, he was supported by the University of California's Regents Fellowship. He is a senior member of the IEEE.